NMR IN BIOMEDICINE
NMR Biomed. 2008; **21**: 217–225
Published online 7 June 2007 in Wiley InterScience
(www.interscience.wiley.com) DOI:10.1002/nbm.1184

Reinvestigating hyperpolarized ^{129}Xe longitudinal relaxation time in the rat brain with noise considerations

X. Zhou,[1]* M. L. Mazzanti,[1] J. J. Chen,[2] Y.-S. Tzeng,[1] J. K. Mansour,[1] J. D. Gereige,[1] A. K. Venkatesh,[1] Y. Sun,[1] R. V. Mulkern[1] and M. S. Albert[1]

[1]Department of Radiology, Brigham and Women's Hospital, Harvard Medical School, Boston, MA 02115, USA
[2]Research Laboratory of Electronics, Massachusetts Institute of Technology, Cambridge, MA 02139, USA

Received 20 January 2007; Revised 18 April 2007; Accepted 18 April 2007

ABSTRACT: The longitudinal relaxation time of hyperpolarized (HP) ^{129}Xe in the brain is a critical parameter for developing HP ^{129}Xe brain imaging and spectroscopy and optimizing the pulse sequences, especially in the case of cerebral blood flow measurements. Various studies have produced widely varying estimates of HP ^{129}Xe T_1 in the rat brain. To make improved measurements of HP ^{129}Xe T_1 in the rat brain and investigate how low signal-to-noise ratio (SNR) contributes to these discrepancies, we developed a multi-pulse protocol during the washout of ^{129}Xe from the brain. Afterwards, we applied an SNR threshold theory to both the multi-pulse protocol and an existing two-pulse protocol. The two protocols yielded mean $\pm$ SD HP ^{129}Xe T_1 values in the rat brain of 15.3 ± 1.2 and 16.2 ± 0.9 s, suggesting that the low SNR might be a key reason for the wide range of T_1 values published in the literature, a problem that might be easily alleviated by taking SNR levels into account. Copyright © 2007 John Wiley & Sons, Ltd.

KEYWORDS: hyperpolarized ^{129}Xe; longitudinal relaxation time; rat; brain; signal-to-noise ratio (SNR)

INTRODUCTION

Since hyperpolarized (HP) ^{129}Xe MRI was first demonstrated in the lung (1), air space imaging using HP noble gases (^{129}Xe and ^{3}He) has progressed at a rapid rate. Owing to high lipid solubility, absence of background signal in biological tissue, non-invasiveness, and lack of radioactivity (2), HP ^{129}Xe MRI has great potential as a tool for studying the brain (3–5), especially for the assessment of cerebral blood flow (CBF) (6). For conventional MRI, the magnetization at thermal equilibrium is induced by the magnetic field, and the longitudinal relaxation time (T_1) is the time for the magnetization, i.e. the MR signal, to recover to thermal equilibrium. However, HP gas magnetization enhanced by spin-exchange optical pumping (7–10) is non-recoverable, and the T_1 of an HP gas is the time elapsed for the signal to decay, because its equilibrium polarization is almost zero relative to the HP polarization. Thus, a 90° pulse would totally consume the HP magnetization. Usually, small flip angles must be used to ration the HP magnetization, and it is very important to have as long a T_1 as possible to ensure that the signal lasts long enough for the acquisition. Therefore, when considering HP ^{129}Xe as a marker for brain perfusion by MRI, evaluation of tissue characterization and pulse sequence optimization, the T_1 of HP ^{129}Xe in the brain is a critical parameter. Previous attempts to measure T_1 in the rat brain have yielded strikingly disparate results. Wilson *et al*. (11) found that T_1 measured in rat brain homogenates *in vitro* ranged from 18 ± 1 to 22 ± 2 s (mean $\pm$ SD) depending on the oxygenation level of the tissue, and T_1 values from measurements in rat brain *in vivo* have ranged from 3.6 ± 2.1 (12) to 26 ± 4 s (13). Part of the discrepancy is believed to be due to the protocols used in T_1 determination. The attempt of Choquet *et al*. (12) used a multi-pulse protocol during the uptake and washout process by injecting HP ^{129}Xe in a lipid emulsion, whereas the estimation of Wakai *et al*. (13) used a two-pulse protocol during the washout process after the rat had breathed HP ^{129}Xe gas. Under the condition of typically achieved polarizations (5–21%) (14), low signal-to-noise ratio (SNR) due to the low concentration of the dissolved HP ^{129}Xe in tissue is an important factor in making T_1 measurements in the rat brain (2,15). The maximum SNR in the above two measurements *in vivo* was only 30 (12) and 46 (13), and the noise effect was not considered in these studies. When the SNR is low, noise will dominate the measured signal and result in large

**Correspondence to:* X. Zhou, Department of Radiology, Brigham and Women's Hospital, Harvard Medical School, 221 Longwood Avenue, Room 010F, Boston, MA 02115, USA.
E-mail: dr.xin.zhou@gmail.com
Contract/grant sponsor: National Aeronautics and Space Administration; *contract/grant number:* NAG9-1469.
Contract/grant sponsor: General Electric Healthcare.

Abbreviations used: CBF, cerebral blood flow; CSI, chemical shift image; FID, free induction decay; HP, hyperpolarized; RF, radio frequency; SNR, signal-to-noise ratio.

differences between the true T_1 and the measured T_1. Thus, low SNR might be a large contributor of error in the published T_1 values.

In this study, we investigated the error in T_1 measurement as a result of low SNR of the ^{129}Xe signal *in vivo*. Correcting for these errors allowed us to more accurately measure the T_1 of HP ^{129}Xe in the rat brain *in vivo*. Our calculations produced highly consistent T_1 results independent of the measurement protocol and offer a resolution to the discrepancy between previously reported values.

MATERIALS AND METHODS

Production of HP ^{129}Xe gas

^{129}Xe gas was hyperpolarized by spin-exchange optical pumping (7–10). A commercially built HP noble gas flow-through system (IGI.XE.2000; Amersham Health, Durham, NC, USA) was used in these studies. The 794.7 nm laser light, from a 60 W diode laser array, resonates with the Rb D1 transition line and induces an electron spin polarization in the Rb vapor via a standard optical pumping process. An initial gas mixture of 1% natural abundance xenon, 10% nitrogen, and 89% helium was introduced into the glass optical cell of the polarizer at ~5 atm. The nitrogen gas was used to quench the fluorescence of Rb atoms for production of the highly polarized ^{129}Xe gas, and the helium is intended to pressure-broaden the Rb D1 profile in order to absorb most of the laser power. The HP ^{129}Xe gas was then produced by spin-exchange collision with the optically pumped Rb atoms. The resulting HP ^{129}Xe was subsequently cryogenically stored in a cold trap with liquid nitrogen at 77 K. With this procedure, 500 mL HP ^{129}Xe gas with a polarization level of ~10% can be obtained in 45 min. After collection, the xenon is warmed and expanded into a Tedlar bag at room temperature, where the longitudinal relaxation time is about 1.5 h.

Animal procedures and HP ^{129}Xe delivery

All animal procedures were approved by the Harvard Medical Area Standing Committee on Animals. Six male Sprague–Dawley rats weighing 175–230 g were used. Each rat was initially anesthetized by intraperitoneal injection of ketamine (24 mg/kg) and xylazine (6 mg/kg), and catheterization into the trachea was performed with a 14-gauge 3.5 cm catheter. Afterwards, the rat was promptly placed in the magnet and the catheter was connected to an animal respirator (SAR 830 AP; CWE Inc., Ardmore, PA, USA), which was interfaced to an MR-compatible gas delivery system controlled via computer software (LabView; National Instruments, Austin, TX, USA). All gases, including HP ^{129}Xe gas, were delivered to the animal through the delivery system, which was especially designed to minimize polarization loss during transportation of the polarized gas (16). The rat was ventilated with 97% O_2 and 3% isoflurane, in order to maintain anesthesia throughout the entire experimental procedure, at 60 breaths per min. A tidal volume of 3 mL was supplied for each breath. Immediately before acquisition of dynamic spectra of the rat brain, the animal was ventilated with alternate breaths of 97% O_2 + 3% isoflurane (2 s) and 100% HP ^{129}Xe gas (2 s) for 40 s. During both surgery and MR scans, body temperature was maintained at 37°C using a water-jacket-type heating pad. The blood oxygenation and heart rate of the animal were monitored using a pulse oximeter (8600 V; Nonin Medical Inc., Plymouth, MN, USA) via a pair of photo transducers placed on the hind paw during the entire experimental procedure.

Multi-pulse and two-pulse washout protocols

HP ^{129}Xe transport in the brain has been modeled using appropriate adaptations of the Kety–Schmidt theory (17,18). The following equation has been derived by Martin *et al*. (17) for the cerebral xenon concentration during HP ^{129}Xe delivery to the lungs:

$$\frac{dC_{brain}}{dt} = FC_{cereb} - \left(\frac{F}{p} + \frac{1}{T_{1brain}}\right)C_{brain}, \qquad (1)$$

where C_{cereb} is the xenon concentration in the cerebral artery, C_{brain} is the xenon concentration in brain parenchyma, F is the tissue perfusion in units of (volume blood)/(volume tissue)/time, p is the brain/blood partition coefficient for xenon, and T_{1brain} is the longitudinal relaxation time of xenon in the brain. In this equation, the first term on the right describes xenon transport to the brain and the second term describes the loss of xenon from the brain by perfusion as well as signal loss caused by T_1 decay. Xenon signal observed from the brain is proportional to C_{brain}. During the washout phase of the xenon signal, there is no transport of HP ^{129}Xe by the cerebral artery, and hence C_{cereb} is zero. The xenon concentration in the brain during washout ($C_{brainwashout}$) is given by the following equation:

$$\frac{dC_{brainwashout}}{dt} = -\left(\frac{F}{p} + \frac{1}{T_{1brain}}\right)C_{brainwashout}. \qquad (2)$$

This equation can be solved to yield an analytical solution for the concentration of xenon in the rat brain during the washout of signal. The decay time constant (τ) of HP ^{129}Xe during the washout from the rat brain is given by:

$$\tau = \frac{1}{\left(\frac{F}{p} + \frac{1}{T_{1brain}}\right)}. \qquad (3)$$

Thus, τ can be calculated from a series of pulse excitations (multi-pulse protocol) after compensating for the HP xenon signal losses caused by radio frequency

DOI: 10.1002/nbm

(RF) excitation, as described below. To compare the results obtained using the multi-pulse protocol, a two-pulse protocol has also been adopted to measure τ (13). Both protocols were performed on each rat during the washout phase of the ^{129}Xe signal.

NMR methods

All MR measurements from the rat brain were carried out on a Bruker Biospec 4.7 T MRI system using a dual-tuned surface coil (3.5 cm diameter) tuned to the ^{1}H and ^{129}Xe resonance frequencies (200.1 and 55.4 MHz, respectively). Shimming was implemented on the proton signal from the rat brain by using the automatic shimming tools (Bruker Paravision 3.0.2). To guarantee the quality of shimming from one experiment to another, the full width at half maximum of the HP ^{129}Xe spectroscopy peak at 194.7 ppm was always shimmed to about 58 Hz. First, a typical ^{129}Xe MR image of the rat brain was obtained by averaging 50 acquisitions in order to identify the chemical shift of the dissolved-phase HP ^{129}Xe in the rat brain tissue. Immediately afterwards, a HP ^{129}Xe 2D chemical shift image (CSI) was acquired to confirm that this dissolved-phase ^{129}Xe signal did originate from the rat brain tissue, by coregistering with a traditional proton reference image of the rat brain. The HP ^{129}Xe CSI used 16 phase-encoding steps in two dimensions, a phase gradient duration of 500 μs, a flip angle of 10°, a *TR* of 1000 ms, a field of view of 2.5 cm, and a slice thickness of 10 mm. K-space data were zero-padded to yield a reconstructed image of 32×32 pixels. Then, to validate the assumption of the SNR threshold theory (see the Appendix), a noise scan was carried out. Without ventilating the rat with HP ^{129}Xe gas, the MR signal at the ^{129}Xe resonance frequency was obtained from the rat brain with an average of 512 acquisitions. After that, a dynamic scan was performed during the uptake and washout of xenon to ensure that 40 s of administration was enough for xenon to reach a saturated state in the rat brain, and the experimental flip angle ($\theta = 13.5 \pm 0.2°$) was calibrated by the method of Patyal *et al.* (19). Spectroscopic scans using two T_1 protocols (see below) were started 6 s after the end of delivery of HP ^{129}Xe. The 6 s delay was to make sure that the delivery of xenon to the brain had ceased, because xenon residence time in the lung and the transportation time of blood from the lung to the brain are both less than 5 s (20).

In the multi-pulse protocol, eight pulses were applied with a 2 s inter-pulse interval during the washout. As the HP magnetization is non-renewable and the magnetization remaining after n excitation pulses with an RF pulse of flip angle θ is $\cos^n\theta$ (21), the loss of HP ^{129}Xe magnetization due to each RF pulse was corrected for by dividing by a factor of $\cos^n\theta$. In the two-pulse protocol, two pulses were applied with a variable inter-pulse interval (Δt), and no corrections for loss of xenon magnetization due to RF pulses were accounted for (13). Eight scans were carried out using Δt values ranging from 2 s to 16 s in 2 s increments. A hard-pulse sequence, with the RF pulse centered at 200 ppm with respect to the xenon gas peak, was used for all measurements. The bandwidth of measurement was 20 kHz, and the size of acquisition was 2048 complex data points.

Data analysis

Before application of a fast Fourier transform, each free induction decay (FID) was processed using a 20 Hz exponential line-broadening filter. The peak at 194.7 ppm and the other adjacent peaks were fitted using a multi-peaks Lorentzian function, and the integral area of the corresponding Lorentzian fitting was considered to be the xenon signal intensity. For the multi-pulse protocol, the decay time constant was obtained from the slope of the logarithm of the signal magnitude plotted against time. For the two-pulse protocol, the decay time constant was obtained from the slope of the logarithm of the ratio of the two signal magnitudes plotted against the time interval. The above two protocols use a linear equation to fit the logarithm of the signal magnitudes, because linear fitting incurs less error than directly fitting the signal magnitudes using a non-linear exponential equation (22). Decay time constants from both protocols were used to calculate T_{1brain} values with eqn (3), and T_{1brain} of HP ^{129}Xe was obtained using both protocols employing standard literature values of 106 ± 7 mL/100 g/min for the normal CBF in the rat and 1.015 for the partition coefficient of ^{129}Xe in the brain (23). For each protocol, all data points were fitted (conventional method). In a second analysis, only the data with SNR > 5.5 (improved method) were fitted on the basis of the SNR threshold theory (see the Appendix). The threshold SNR of 5.5 was selected to ensure agreement of less than 5% error between the measured and actual signal in the T_1 experiments.

Four groups of T_1 values were obtained from this study, and a statistical analysis of variance was conducted between these groups. Comparisons were made for T_1 values computed using the conventional approach as well as the SNR threshold approach for both protocols to examine if SNR has an effect. The T_1 values computed with SNR considerations using the two protocols were also compared to examine whether accounting for SNR would lead to a consistency between protocols. Statistical significance was set at $P < 0.05$ for evaluating mean differences between groups of T_1 values.

RESULTS AND DISCUSSION

When xenon administration was initiated, the blood oxygenation of the rats fell from 99–100% to 92–93% for

DOI: 10.1002/nbm

the first 20–25 s. After that, it recovered to 99–100% in 5–10 s, and remained at this level for the entire experiment, even in the two-pulse protocol experiments with a 560 s duration. The heart rates of the different rats ranged from 210 to 250. Figure 1 shows a typical ^{129}Xe MR spectrum obtained from the brain of rat 2 *in vivo*. The HP ^{129}Xe gas peak was set as 0 ppm for reference. The two clearly prominent peaks at 194.7 ppm and 189 ppm were identified as dissolved HP ^{129}Xe in the brain tissue and non-brain tissue, respectively, and a broad peak around 209.5 ppm was identified as dissolved HP ^{129}Xe in the blood, on the basis of the results of Nakamura *et al*. (20). The identities of the smaller peaks at 191.6 ppm and 197.8 ppm are still unknown and remain to be determined. That the signal at 194.7 ppm originated from the brain tissue can be confirmed because the HP ^{129}Xe CSI at 194.7 ppm coregistered very well with a traditional proton image in the brain, as shown in Fig. 2. This CSI looks heterogeneous, which may be due to the perfusion differences of the complex structures of the rat brain, and the combination of different structures of the 10 mm slice thickness. The ratio of white matter to gray matter in the rat brain is about 1:4, which is much lower than that in humans (approximately 3:2). Also perfusion and other physiological parameters are very different in the rat brain compared with the human brain. During a total CSI acquisition time of 256 s, the perfusion differences between the white and gray matter and the different structures of the 10 mm thick slices excited by a non-selective RF pulse might lead to the inhomogeneous distribution of 194.7 ppm peak signal intensity in the CSI, which remains to be further investigated. Although the high-quality MRS of the brain obtained *in vivo* shows five peaks, the HP ^{129}Xe signal from the rat brain tissue was overwhelmingly dominated by the single resonance at 194.7 ppm.

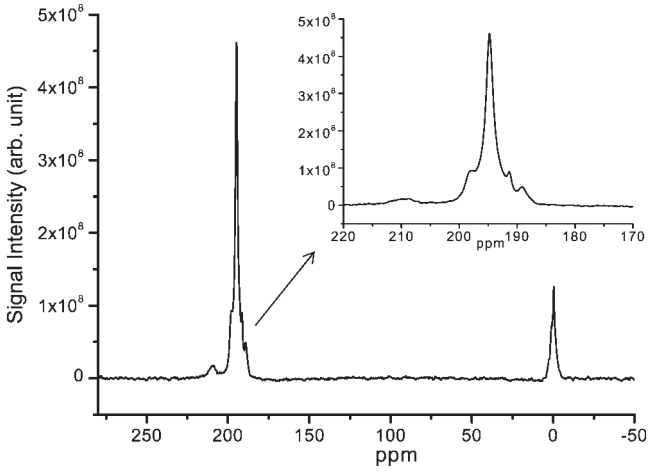

Figure 1. Typical ^{129}Xe MRS of the rat brain *in vivo*. With respect to the gas resonance (0 ppm), five dissolved peaks were observed. A dominant peak at 194.7 ppm and another discriminable peak at 189 ppm were identified as dissolved HP ^{129}Xe in the brain tissue and non-brain tissue, respectively. Two small peaks at 191.6 ppm and 197.8 ppm are still unknown, and a smaller broad peak at 209.5 ppm comes from the dissolved HP ^{129}Xe in the blood.

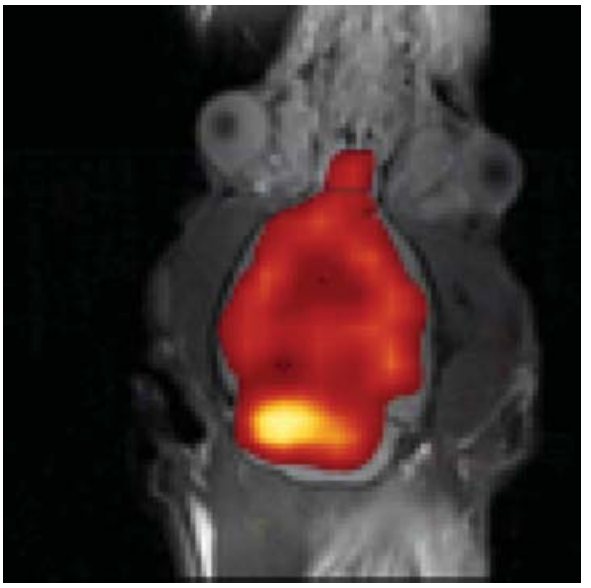

Figure 2. Depiction of HP ^{129}Xe distribution in the rat brain tissue by coregistering the brain HP ^{129}Xe CSI at 194.7 ppm with a proton MR reference image. The proton MRI (grayscale image) corresponds to a 1 mm coronal slice through the brain acquired with a rapid acquisition with relaxation enhancement (RARE) pulse sequence. HP ^{129}Xe CSI of 194.7 ppm resonance frequency (shown as with a false color overlay) acquired with a 2D CSI pulse sequence. The HP ^{129}Xe CSI confirms that the signal at 194.7 ppm originated from the rat brain tissue.

For the noise scan, both the arithmetic means of the real and imaginary parts of signals at 194.7 ppm from the rat brain, which was Fourier-transformed from 512 FIDs, were about zero. These peak intensities have been divided into 10 bins, and the corresponding histogram is shown in Fig. 3. It clearly indicates that the noise on the two

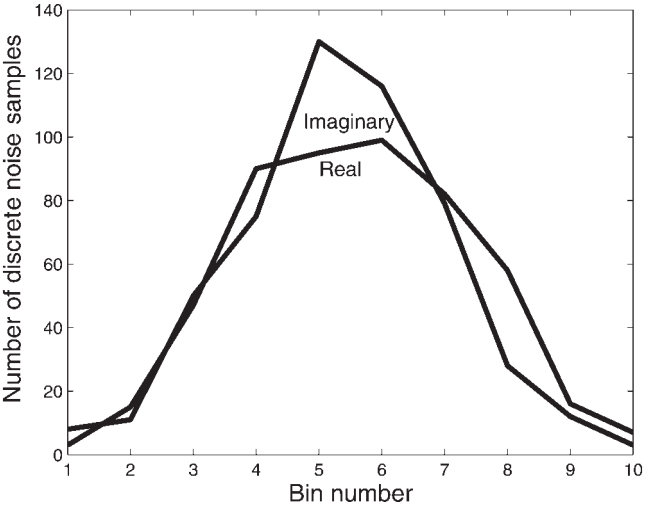

Figure 3. Histogram of peak intensities of 512 noise FIDs at 194.7 ppm was divided into 10 bins, which demonstrates that the noise on the two quadrature detectors is a normal distribution.

DOI: 10.1002/nbm

quadrature detectors are both normal distributions. Because a normal noise distribution is required for the application of this SNR threshold theory, the observation that our noise properties do indeed have a normal distribution justifies our utilization of this approach (see the Appendix).

Figure 4 illustrates the dynamic, high-SNR HP ^{129}Xe MR image from the brain of rat 2 during the uptake and washout of HP ^{129}Xe. The dissolved signal in the rat brain clearly reached a steady state at about 30 s after HP ^{129}Xe ventilation began. Therefore, a 40 s time period for alternating breaths of oxygen and HP ^{129}Xe was sufficient for saturation of dissolved-phase xenon in the rat brain. At 44 s, the HP ^{129}Xe signal in the rat brain began to decay, which confirmed that a 6 s delay was sufficient for the delivery of xenon from the lungs to the brain.

Figure 5a shows typical linear fits for all data points (dashed line) and also for the data with SNR $\geq$ 5.5 only (solid line), both obtained using the multi-pulse protocol from rat 2. Figure 5b shows typical linear fits for all data points (dashed line) and only for the data in which spectrum peaks, S_2, have SNR $\geq$ 5.5 (solid line), both from the two-pulse protocol, also from rat 2. Table 1 shows individual T_1 values of HP ^{129}Xe and their mean from the six rat brains using the two protocols, with and without the SNR threshold. These four groups of T_1 values computed will hereafter be referred to as 'group 1' through 'group 4' as indicated in Table 1. To compare the mean values of the four different groups, the LSD (least-significant difference) multiple comparisons using an analysis of variance are shown in Table 2. The mean T_1 values determined using these two protocols differed significantly ($P << 0.05$ between groups 1 and 3) if all the data were fitted without thresholding out the low-SNR data points, i.e. the conventional method. However, if the effect of noise was minimized, i.e. the improved method, the T_1 values computed have a much smaller difference

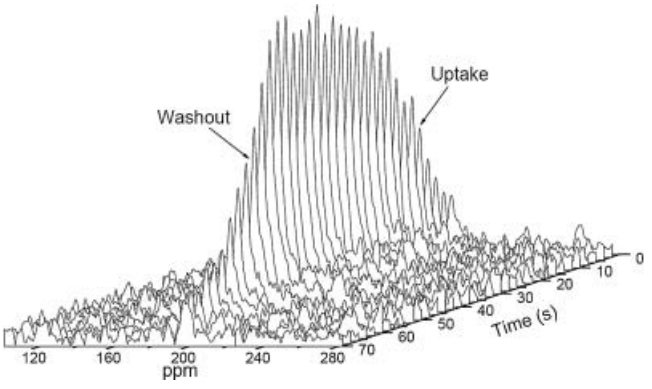

Figure 4. Under the conditions of a 40 s period for alternating breaths of oxygen and HP ^{129}Xe, MRS image of HP ^{129}Xe obtained from rat brain *in vivo* with a dynamic sequence during the uptake and washout of xenon. At about 30 s from the beginning of xenon ventilation, the dissolved ^{129}Xe signal reached a steady state and began to decay at about 44 s.

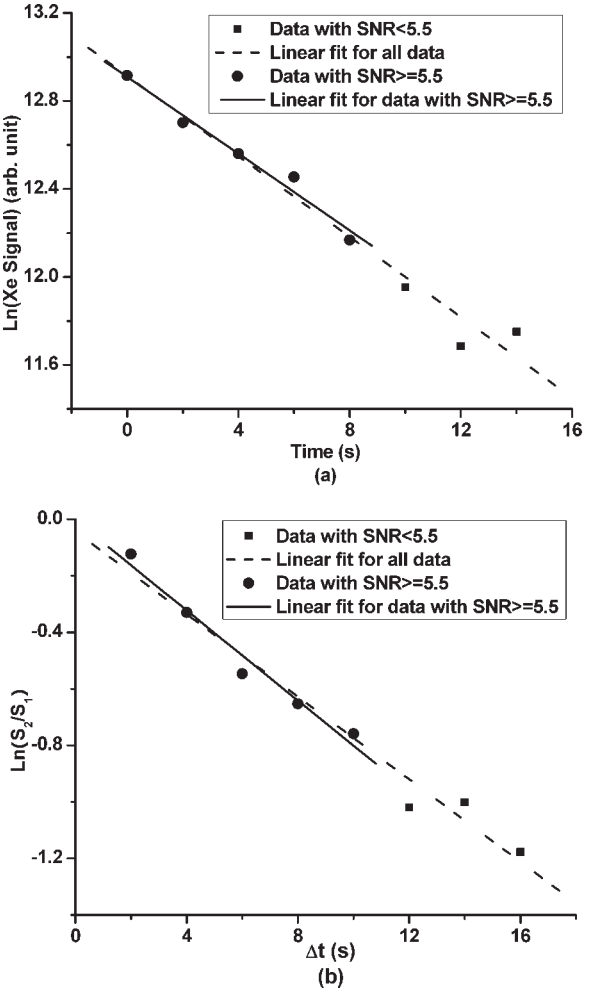

Figure 5. A typical time-dependent decay of HP ^{129}Xe during washout from rat brain using (a) the multi-pulse protocol and (b) the two-pulse protocol. The dashed lines represent the linear fittings for all data points, and the solid lines are the linear fittings for the data with SNR $\geq$ 5.5 only.

Table 1. T_1 values of HP ^{129}Xe from six rat brains. The mean T_1 value and standard deviation obtained from the multi-pulse and two-pulse protocols before (conventional method) and after (improved method) setting a threshold for SNR are also given. These T_1 values were named 'group 1' to 'group 4' for easy reference during discussion

	Multi-pulse protocol		Two-pulse protocol	
	Conventional	Improved	Conventional	Improved
Rat	T_1(s) (group 1)	T_1(s) (group 2)	T_1(s) (group 3)	T_1(s) (group 4)
1	14.2	12.9	19.5	17.6
2	12.2	15.1	18.2	16.4
3	11.5	16.1	16.3	14.9
4	11.7	15.5	18.0	16.5
5	12.7	16.4	18.8	16.6
6	12.1	15.7	17.2	15.4
Mean	12.4	15.3	18.0	16.2
SD	1.0	1.2	1.1	0.9

DOI: 10.1002/nbm

Table 2. LSD multiple comparisons using analysis of variance between four T_1 value groups. It shows the mean difference is −5.6 s and $P < 0.05$ between the multi-pulse protocol (group 1) and two-pulse protocol (group 3) when the SNR threshold theory is not used, whereas the mean difference is −0.95 s and $P > 0.05$ between the two protocols (groups 2 and 4) when the SNR threshold theory is applied

Group (I)	Group (J)	Mean difference (I–J)	SE	P value	95% Confidence interval	
					Lower	Upper
1	2	−2.9	0.63	1.8E-04	−4.2	−1.6
3	4	1.8	0.63	1.1E-02	0.5	3.1
1	3	−5.6	0.63	2.1E-08	−6.9	−4.3
2	4	−0.95	0.63	0.146	−2.3	0.4

(−0.95 s between groups 2 and 4) than that using the convention method (−5.6 s between groups 1 and 3). Table 2 also shows that significant differences were found between the T_1 values derived using the conventional and improved multi-pulse methods ($P < 0.05$ between groups 1 and 2) as well as those derived using the conventional and improved two-pulse methods ($P < 0.05$ between groups 3 and 4). However, when the SNR threshold was applied, there was no significant difference between the results using multi-pulse and two-pulse methods ($P > 0.05$ between groups 2 and 4). It supports our hypothesis that the noise does affect the accuracy of the T_1 values to a great extent.

Table 1 shows that the mean T_1 value calculated using the improved two-pulse method is larger than that using its conventional counterpart, whereas the mean T_1 value calculated using the improved multi-pulse method is less than that using its conventional counterpart. The analysis of variance results in Table 2 show that the mean difference between the T_1 values (−2.9 s between groups 1 and 2) calculated using the conventional and improved multi-pulse methods is larger than the mean difference between the T_1 values (1.8 s between groups 3 and 4) calculated using the conventional and improved two-pulse methods. Extending the analysis of Henkelman (24), it was found that noise usually adds a statistically positive bias to low SNR signals, although it could induce a negative bias in an individual scan. When the two-pulse protocol was used, it was reasonable that the T_1 mean value was overestimated when all data points were used, because the T_1 value was proportional to $\ln(S_2/S_1)$, and, overall, noise would have a larger positive bias on S_2 with a lower SNR. Theoretically, the precision of the T_1 value measured using the two-pulse protocol is dependent only on the noise content of the acquired signals; however, the same parameter measured using the multi-pulse protocol is further reliant on the accuracy of the flip angle. For the results from the multi-pulse protocol, the underestimation of the T_1 mean value using the conventional method relative to the improved method may be due to the error of the calibration of the flip angle. To correct for the effect of the flip angle, the acquired signals were divided by a factor of $\cos^n\theta$. These corrected signal levels were then used to calculate T_1. Therefore, an overestimation of $\cos\theta$ might lead to the underestimation of T_1 values, and errors from misestimating $\cos^n\theta$ can magnify with increasing n. As a surface coil was used for measurements, the RF inhomogeneity of the coil would produce variations in the flip angle profiles. The assumption of $\pm1^\circ$ error of flip angle determination would induce ±1 s and ±0.8 s errors in the final T_1 mean values computed by the multi-pulse conventional and improved methods, respectively. If the incertitude on the flip angle were $\pm2^\circ$, the errors of the T_1 mean values would merely increase to ±1.6 s and ±1.3 s for the multi-pulse conventional and improved methods.

From eqn (3), we know that the accuracy of the T_1 values depends on how close the CBF and partition coefficient of our rats are to those values reported in the literature. An overestimation of the CBF would result in an overestimation of the T_1 value, and an overestimation of the partition coefficient would induce an underestimation of the T_1 value. As for the CBF, it might change with physiological interventions (e.g. anesthesia) and would vary between individual animals. It was reported that the CBF varied from 66 to 117 mL/100 g/min in normorcapnia (23) and up to 131 ± 9 mL/100 g/min when iodo-[^{14}C]antipyrine was used (25). Assuming that the partition coefficient remains constant at 1.015 if the CBF were as low as 66 mL/100 g/min, the mean T_1 values would decrease to 13.9 s and 14.6 s when the improved multi-pulse and improved two-pulse protocols, respectively, were used. These mean T_1 values would increase to 16.3 s and 17.4 s assuming that the CBF is 131 ± 9 mL/100 g/min. As for the effect of variations in the partition coefficient on the accuracy of the T_1 measurements, using CBF from the standard literature (106 ± 7 mL/100 g/min), a $\pm5\%$ difference in the partition coefficient would only induce a ±0.2 s difference in the mean T_1 values using either the improved multi-pulse or the improved two-pulse protocols. The goal of this paper, however, is to demonstrate that the accuracy of T_1 results can be improved once the SNR threshold theory is applied to two measurement protocols. An independent measurement of the CBF and partition coefficient made simultaneously with xenon washout would more accurately determine the T_1 values based on our methods.

As the T_1 values in the rat brain were determined by Choquet *et al*. (12) using data that included the uptake process of HP ^{129}Xe gas, the fluctuation of xenon concentration in the rat brain caused by the manual injection of HP ^{129}Xe in a lipid emulsion may introduce a large error. Moreover, those data were fitted using a complicated multi-exponential equation, which may also lead to a larger error than that expected using linear fitting. Wakai *et al*. (13) did not clearly describe how HP

DOI: 10.1002/nbm

^{129}Xe was administered to the rat, whether the breaths contained a mixture of HP ^{129}Xe and oxygen, or whether alternate breaths of HP ^{129}Xe and oxygen were used. In any case, although 91% enriched ^{129}Xe gas was used, the best data in their study had an SNR of only 46. In addition, a large error may exist in the estimated decay time because the two-pulse protocol is sensitive to the SNR of the spectra.

In contrast with the above two studies, because our experiment determined the T_1 value only via the washout phase, it was independent of fluctuations in xenon concentration during the uptake process and avoided the unnecessary associated error. Also, it was relatively easy to identify the washout phase, as the data at a fixed time (6 s) after the end of xenon delivery (allowing for the xenon transit time to the brain) were selected for measurement of the decay time constant. Furthermore, the rats in our experiments were ventilated with alternating breaths of HP ^{129}Xe and oxygen by a computer-controlled delivery system, so the depolarization of HP ^{129}Xe should be slower than that using breaths of HP ^{129}Xe mixed with oxygen. Even though only natural abundance xenon was used in our experiment, our data consistently had an SNR > 61. Therefore, our procedure should provide a better basis for accurate measurement of T_1 in the rat brain.

In two previous studies (12,13), the T_1 values were very sensitive to the SNR, regardless of which T_1 measurement protocol was used. In our study, we confirmed by using two different measurement protocols and applying the SNR threshold theory that one of the large sources of error in the two previous studies was noise. Our results demonstrate that noise influences the measured T_1 value accuracy to a large degree when the signal SNR is low. Quantitatively, there is more than a 5% difference between the true signal and the measured signal if the SNR is less than 5.5.

The two approaches used in the present study each have their own strengths and weaknesses. The multi-pulse protocol, all in all, takes 70 s. Sufficient data are acquired to calculate T_1 within the washout period during the latter period of ~24 s. However, the fidelity of the multi-pulse protocol depends on both the inhomogeneity and the accuracy of the delivered flip angle. We chose to use the surface coil for this experiment because of its higher signal sensitivity than the birdcage coil. However, we acknowledge that the surface coil is inferior to the birdcage coil in terms of RF field homogeneity. Even if we had chosen to use a birdcage coil, we cannot be certain that the reduction in errors due to RF field non-uniformity would have been worth the poorer SNR and increased contamination from signal originating nearby. Fortunately, the flip angles can be easily and quickly calibrated in less than 1 s, and the larger error from $\cos^n\theta$ when n is large can be circumvented by discarding the later data points with SNR < 5.5. For the two-pulse protocol, inhomogeneous RF field distribution can be avoided because the flip angle need not be estimated. However, the two-pulse protocol is more time consuming (at least 560 s in the current protocol) as it requires eight repetitions to collect a full dataset. Moreover, the polarization loss over such a long period results in lower SNR values for the later data points. Nonetheless, we used these two different protocols and proved that the T_1 value results were consistent once the noise effect had been accounted for by utilizing the SNR threshold theory.

CONCLUSION

To our knowledge, the noise effect has not been considered in previous studies measuring ^{129}Xe T_1 in the brain. Because the concentration of HP ^{129}Xe in brain tissue is typically low, it follows that the SNR of the MR signal from the brain will be low as well, although methods for increasing polarization levels should ameliorate this somewhat (26). We reinvestigated the HP ^{129}Xe T_1 in the rat brain *in vivo* incorporating noise/SNR considerations, and although numerous physical and physiological factors may affect the T_1 obtained, our approach supports our hypothesis that noise has an undeniable effect on the accuracy of T_1 measurements. This study demonstrates an improvement when the influence of noise is minimized.

With the assistance of high SNR, by incorporating an SNR threshold into two different MRS approaches, the T_1 mean values of HP ^{129}Xe in the rat brain were determined to be 15.3 ± 1.2 and 16.2 ± 0.9 s, respectively, which are highly consistent (0.9 s difference). However, our values do depend on assuming a literature value for CBF in rat brain, which sets a limit on the accuracy of the measurement.

Acknowledgements

This work was funded in part by grants from the National Aeronautics and Space Administration (NAG9-1469) and from General Electric Healthcare.

REFERENCES

1. Albert MS, Cates GD, Driehuys B, Happer W, Saam B, Springer CS Jr, Wishnia A. Biological magnetic resonance imaging using laser-polarized ^{129}Xe. *Nature* 1994; **370**(6486): 199–201.
2. Cherubinia A, Bifone A. Hyperpolarised xenon in biology. *Progress in Nuclear Magnetic Resonance Spectroscopy* 2003; **42**: 1–30.
3. Mugler JP III, Driehuys B, Brookeman JR, Cates GD, Berr SS, Bryant RG, Daniel TM, de Lange EE, Downs JH III, Erickson CJ, Happer W, Hinton DP, Kassel NF, Maier T, Phillips CD, Saam BT, Sauer KL, Wagshul ME. MR imaging and spectroscopy using hyperpolarized ^{129}Xe gas: preliminary human results. *Magn. Reson. Med.* 1997; **37**(6): 809–815.

DOI: 10.1002/nbm

4. Swanson SD, Rosen MS, Agranoff BW, Coulter KP, Welsh RC, Chupp TE. Brain MRI with laser-polarized ^{129}Xe. *Magn. Reson. Med.* 1997; **38**(5): 695–698.
5. Albert MS, Venkatesh AK, Li LP, Chin Cl, Balamore D, Jolesz FA. Dynamic uptake of hyperpolarized ^{129}Xe in the rat brain. *Eur. Radiol.* 1999; **38**: B41.
6. Duhamel G, Choquet P, Grillon E, Leviel JL, Decorps M, Ziegler A, Constantinesco A. Global and regional cerebral blood flow measurements using NMR of injected hyperpolarized xenon-129. *Acad. Radiol.* 2002; **9** (Suppl. 2): S498–S500.
7. Walker TG, Happer W. Spin-exchange optical pumping of noble-gas nuclei. *Reviews of Modern Physics* 1997; **69**: 629–642.
8. Zeng X, Wu Z, Call T, Miron E, Schreiber D, Happer W. Experimental determination of the rate constants for spin exchange between optically pumped K, Rb, and Cs atoms and ^{129}Xe nuclei in alkali-metal-noble-gas van der Waals molecules. *Phys. Rev. A* 1985; **31**: 260–278.
9. Zhou X, Luo J, Sun X, Zeng X, Wu S, Liu M, Zhan M. Enhancement of solid-state proton NMR via the spin-polarization-induced nuclear Overhauser effect with laser-polarized xenon. *Phys. Rev. B* 2004; **70**: 052405.
10. Zhou X, Sun X, Luo J, Zeng X, Liu M, Zhan M. Production of hyperpolarized ^{129}Xe gas without nitrogen by optical pumping at ^{133}Cs D_2 Lin in flow system. *Chinese Physics Letters* 2004; **21**: 1501–1503.
11. Wilson GJ, Santyr GE, Anderson ME, DeLuca PM Jr. Longitudinal relaxation times of ^{129}Xe in rat tissue homogenates at 9.4 T. *Magn. Reson. Med.* 1999; **41**(5): 933–938.
12. Choquet P, Hyacinthe JN, Duhamel G, Grillon E, Leviel JL, Constantinesco A, Ziegler A. Method to determine *in vivo* the relaxation time T_1 of hyperpolarized xenon in rat brain. *Magn. Reson. Med.* 2003; **49**(6): 1014–1018.
13. Wakai A, Nakamura K, Kershaw J, Kondoh Y, Wright D, Kanno I. A method for measuring the decay time of hyperpolarized ^{129}Xe magnetization in rat brain without estimation of RF flip angles. *Magn. Reson. Med. Sci.* 2005; **4**(1): 19–25.
14. Zook AL, Bowers CR. High capacity production of >40% spin polarized xenon-129 for NMR and MRI applications at the NHMFL. *Laboratory Spotlight*. Reprinted from NHMFL Reports, Fall 2001.
15. Ruppert K, Brookeman JR, Hagspiel KD, Mugler JP III. Probing lung physiology with xenon polarization transfer contrast (XTC). *Magn. Reson. Med.* 2000; **44**(3): 349–357.
16. Venkatesh AK, Zhao L, Pausak T, Ward CF, Jolesz FA, Albert MS. Hyperpolarized gas imaging using a simple programmable gas delivery system. *Eur. Radiol.* 1999; **9**: B34.
17. Martin CC, Williams RF, Gao JH, Nickerson LD, Xiong J, Fox PT. The pharmacokinetics of hyperpolarized xenon: implications for cerebral MRI. *J. Magn. Reson. Imag.* 1997; **7**(5): 848–854.
18. Peled S, Jolesz FA, Tseng CH, Nascimben L, Albert MS, Walsworth RL. Determinants of tissue delivery for ^{129}Xe magnetic resonance in humans. *Magn. Reson. Med.* 1996; **36**(3): 340–344.
19. Patyal BR, Gao JH, Williams RF, Roby J, Saam B, Rockwell BA, Thomas RJ, Stolarski DJ, Fox PT. Longitudinal relaxation and diffusion measurements using magnetic resonance signals from laser-hyperpolarized ^{129}Xe nuclei. *J. Magn. Reson.* 1997; **126**(1): 58–65.
20. Nakamura K, Kondoh Y, Wakai A, Kershaw J, Wright D, Kanno I. ^{129}Xe spectra from the heads of rats with and without ligation of the external carotid and pterygopalatine arteries. *Magn. Reson. Med.* 2005; **53**(3): 528–534.
21. Zhao L, Mulkern R, Tseng CH, Williamson D, Patz S, Kraft R, Walsworth RL, Jolesz FA, Albert MS. Gradient-echo imaging considerations for hyperpolarized ^{129}Xe MR. *J. Magn. Reson. B* 1996; **113**: 179–183.
22. Vonesh EF, Chinchilli VM. *Linear and Nonlinear Models for the Analysis of Repeated Measurements*. Marcel Dekker: New York, 1996.
23. Gjedde A, Caronna JJ, Hindfelt B, Plum F. Whole-brain blood flow and oxygen metabolism in the rat during nitrous oxide anesthesia. *Am. J. Physiol.* 1975; **229**(1): 113–118.
24. Henkelman RM. Measurement of signal intensities in the presence of noise in MR images. *Med. Phys.* 1985; **12**(2): 232–233.
25. Sakurada O, Kennedy C, Jehle J, Brown JD, Carbin GL, Sokoloff L. Measurement of local cerebral blood flow with iodo-[^{14}C]antipyrine. *Am. J. Physiol.* 1978; **234**(1): H59–H66.
26. Ruset IC, Ketel S, Hersman FW. Optical pumping system design for large production of hyerpolarization ^{129}Xe. *Phys. Rev. Lett.* 2006; **96**(5): 053002.

APPENDIX

SNR THRESHOLD THEORY

In an MR measurement, suppose A is the true amplitude of the signal and N is the noise, and A can always be chosen to be the real component of the MRI signal by rotating the quadrature detectors. Then, the measured signal including noise can be given using the complex expression:

$$S = A + N_r + iN_i. \quad (4)$$

Assume that the noise on the two quadrature detectors is white, has a normal distribution, and is independent with zero mean and standard deviation σ. The joint probability distribution of the noise can be written as:

$$P(N_r, N_i) = \exp[-(N_r^2 + N_i^2)/2\sigma^2]dN_r dN_i/2\pi\sigma^2, \quad (5)$$

Therefore, the root mean square (RMS) of the measured signal magnitude can be calculated as follows:

$$M_{rms} = \sqrt{\int_{-\infty}^{\infty}\int_{-\infty}^{\infty} |S|^2 P(N_r, N_i)} = \sqrt{2\sigma^2 + A^2}. \quad (6)$$

When $A = 0$, i.e. no signal, the RMS of the noise magnitude is given by $\sqrt{2}\sigma$. In addition, from the definition of SNR:

$$SNR = \frac{P_{signal}}{P_{noise}} = \left(\frac{M_{rms}^{Signal}}{M_{rms}^{noise}}\right)^2, \quad (7)$$

where P is average power and M is RMS amplitude. After inserting eqn (6) into the above equation [7], we can get the measured signal SNR:

$$SNR = \frac{2\sigma^2 + A^2}{2\sigma^2} = 1 + \frac{A^2}{2\sigma^2}. \quad (8)$$

In a similar way to deducing eqn (6), M_{mean}, the arithmetic mean of the measured signal magnitude, can be written in polar coordinates (24):

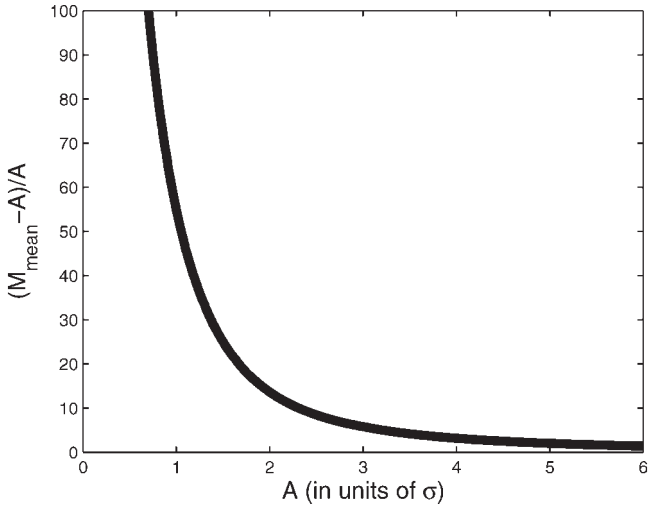

Figure 6. Dependence of $(M_{\text{mean}}-A)/A$, the difference between the arithmetic mean of the measured signal (M_{mean}) and the true signal amplitude (A), on A in units of σ. It shows that when $A > 3$, $(M_{\text{mean}}-A)/A < 5\%$, which means that the measured signal approaches the true signal with an error of less than 5%.

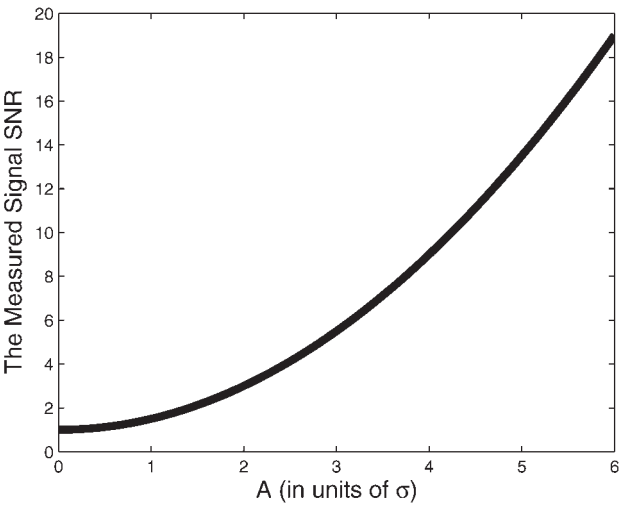

Figure 7. Dependence of the measured signal SNR on the true signal amplitude (A) in units of σ. The measured signal SNR is 5.5 when A is equal to 3σ, which indicates that when the SNR > 5.5, A can be approximated by M_{mean} to an accuracy of better than 5%.

$$M_{mean} = \frac{1}{2\pi\sigma^2}\int_0^{\infty}\int_0^{2\pi}\sqrt{\eta^2 + A^2 + 2\eta A\cos\theta}\,\exp(-\eta^2/2\pi\sigma^2)\eta d\theta d\eta. \quad (9)$$

As the analytical expression of M_{mean} cannot be easily obtained through the above complicated integral, we can numerically evaluate it for $\sigma = 1$, as previously (24). According to the relationship between the arithmetic mean, the standard deviation and the RMS

$$M_{rms}^2 = M_{mean}^2 + M_{sd}^2, \quad (10)$$

M_{sd}, the standard deviation of the measured signal magnitude, can also be derived. For convenience, Fig. 6 shows $(M_{mean}-A)/A$, the difference between the measured mean M_{mean} and the true signal A relative to A, in units of σ. This figure clearly demonstrates that $(M_{mean}-A)/A < 5\%$ when $A > 3\sigma$. The measured signal SNR which depends on the true amplitude A in units of σ is plotted in Fig. 7 according to eqn (8). When $A = 3\sigma$, the measured signal SNR $= 5.5$, which indicates that when SNR > 5.5, A can be approximated by M_{mean} to an accuracy of better than 5%. Therefore, we chose an SNR threshold of 5.5 to decrease the errors stemming from low SNR measurements.

DOI: 10.1002/nbm